Distribution and photoreactivity of chromophoric dissolved organic matter in the Antarctic Peninsula (Southern Ocean)

E. Ortega-Retuerta [a,b,*], I. Reche [a,b], E. Pulido-Villena [c], S. Agustí [d], C.M. Duarte [d]

[a] Departamento de Ecología, Facultad de Ciencias, Universidad de Granada, 18071 Spain
[b] Instituto del Agua, Universidad de Granada, 18071 Spain
[c] Laboratoire d'Océanographie de Villefranche CNRS-UMR 7093, 06238 Villefranche-sur-mer, France
[d] Instituto Mediterráneo de Estudios Avanzados, CSIC-UIB, Miquel Marqués 21, Esporles, Illes Balears, Spain

ARTICLE INFO

ABSTRACT

Chromophoric dissolved organic matter (CDOM) plays a key role regulating light attenuation in the ocean. This optically reactive pool of organic matter is driven by several physical and biological processes such as photobleaching, photohumification, and biogeneration, that act as primary sinks and sources of CDOM. In this study, we described the geographical and vertical distribution of CDOM in the Antarctic Peninsula area (Southern Ocean), and assessed its potential driving factors, with special emphasis on CDOM photoreactivity. CDOM values were between the detection limit and 2.17 m^{-1} at 325 nm and between the detection limit and 0.76 m^{-1} at 443 nm (average $a_{325} = 0.36 \pm 0.02$ m^{-1}, average $a_{443} = 0.11 \pm 0.01$ m^{-1}), with the highest values inside Deception Island in 2004, and the lowest in the Eastern Bransfield Strait. In Bellingshausen Sea, CDOM was higher below the mixed layer suggesting a significant role of photobleaching. By contrast in the Weddell Sea maximum values were found within the mixed layer. In the Weddell Sea, a positive correlation between CDOM and both chlorophyll a and bacterial production and a negative correlation with salinity suggest a biological source of CDOM likely associated to ice melting. Salinity was also negatively related to the spectral slopes from 275 to 295 nm, considered a good proxy for DOM molecular weight. The experimental results demonstrate the photoreactive nature of CDOM, with half lives from 2.1 to 5.1 days due to photobleaching in the upper layer and duplication times from 4.9 to 15.7 days due to photohumification, that highlight the highly dynamic nature of CDOM in this area.

© 2009 Elsevier B.V. All rights reserved.

1. Introduction

Chromophoric dissolved organic matter (CDOM) is the optically active component of dissolved organic matter (DOM) (Coble, 2007; Nelson and Siegel, 2002), formed by organic compounds that absorb light at both ultraviolet (UV) and visible wavelengths. This DOM fraction has a strong impact in the cycling of carbon and other elements mediating photochemical reactions (Kieber et al., 1989, 1999; Mopper et al., 1991) and, consequently, modulates light attenuation in the ocean (Bricaud et al., 1981; Kalle, 1966). Therefore, CDOM interferes with satellite estimations of chlorophyll a and primary production (Siegel et al., 2002, 2005).

In the past, several attempts have been made to use CDOM absorbance or fluorescence as a proxy for dissolved organic carbon (DOC) concentration (Blough and del Vecchio, 2002). However, a significant relationship between these parameters has been found only in coastal areas (Vodacek et al., 1997; Ferrari, 2000), where both DOC and CDOM are mostly of terrestrial origin and controlled by the mixing with oceanic waters. By contrast, in the open ocean, a decoupling or even a near-inverse relationship between dissolved organic carbon (DOC) and chromophoric dissolved organic matter (CDOM) has been reported both in time series (Nelson et al., 1998) and in depth profiles (Hansell and Carlson, 2002). These observations reflect that these two pools of organic matter are governed by different sources and sinks or are recycled at different timescales. In the first studies, CDOM was associated to terrestrial compounds, considered as a refractory pool formed essentially by slow-cycling compounds (Williams, 1971). However, its contemporary origin and short residence time are currently recognized (Amon and Benner, 1994; Opsahl and Benner, 1998; Ortega-Retuerta et al., 2009; Santschi et al., 1995) that result in a dynamic balance between generation and removal processes.

The vast majority of organic carbon in open ocean waters has been produced photosynthetically by phytoplankton. This would suggest phytoplankton as the main source of CDOM, and hence coupled distributions of chlorophyll a (chl a) and CDOM (Carder et al., 1989)

* Corresponding author. Present address: UPMC Univ Paris 06/CNRS, UMR 7621, LOBB, Observatoire Océanologique, F-66651, Banyuls/mer, France. Tel.: +33 430192403.
E-mail address: ortega@obs-banyuls.fr (E. Ortega-Retuerta).

would be expected. Satellite images have shown that the distribution of CDOM together with detrital absorption (CDM) mirrors that of chl *a* at the global scale (Siegel et al., 2002). This coupled relationship has been also observed in regional studies with large spatio-temporal scales (Babin et al., 2003, Kitidis et al., 2006). However, the relationship between CDOM and phytoplankton appears to be indirect through subsequent bacterial processing of the DOM released by algae (Cammack et al., 2004; Nelson et al., 1998; Rochelle-Newall and Fisher, 2002). Indeed, the role of bacteria as CDOM producers has been reported both in field (Nelson et al., 1998) and in experimental studies (Biers et al., 2007; Nelson et al., 2004, Ortega-Retuerta et al., 2009).

Regarding CDOM sinks, photobleaching (the loss of absorbance due to the reaction of solar radiation with CDOM), is considered as a relevant process. Several studies have already shown lower CDOM in the surface than below the upper mixed layer (Chen and Bada, 1992; Nelson et al., 1998; Twardowski and Donaghay, 2001). Experimental studies have also reported CDOM absorbance decay kinetics higher than 50% in terms of days. These kinetics have been frequently associated to increases in the spectral slopes (Del Vecchio and Blough, 2002; Reche et al., 2001; Whitehead et al., 2000) and particularly in the slopes between 275 and 295 nm ($S_{275-295}$), a good proxy for DOM molecular weight (Helms et al., 2008). On the other hand, solar radiation can also lead to increases of CDOM, through the transformation of organic compounds such as fatty acids or triglycerides into humic-like substances (Kieber et al., 1997), a process called photohumification. Therefore, CDOM distribution in open oceans will result from the balance between photobleaching, photohumification, and biogeneration.

Polar oceans appear to be enriched in CDOM likely as a result of low solar incident radiation over the whole year, deep mixed layers, and relatively high primary productivity (Siegel et al., 2002). In the Southern Ocean, organisms are exposed to an extreme solar radiation regime, with high UV radiation in comparison to visible (Smith et al., 1992), and the highest dose of UV found at the end of December. Hence, CDOM plays a crucial role in UV and photosynthetically active radiation (PAR) light attenuation (Siegel et al., 2005), and CDOM photoreactions can be expected to be important. In addition, the particular region of the Antarctic Peninsula is currently one of the most vulnerable areas to global warming (Vaughan et al., 2003). Nevertheless, there is a paucity of studies on CDOM distribution in the Southern Ocean, which are limited to the Australian sector (Clementson et al., 2001) and Ross Sea (Barbini et al., 2003; Misic et al., 2006), with scarce information available on CDOM in the Antarctic peninsula area (Patterson, 2000, Yocis et al., 2000).

In this study, we report geographic and vertical distribution of CDOM around the Antarctic Peninsula (Southern Ocean) and assess its potential driving factors with a special emphasis on CDOM photoreactivity.

2. Material and methods

2.1. Study area and sampling

Sampling was carried out during January and February 2004 and 2005 in the two ICEPOS oceanographic cruises along the Antarctic Peninsula and Bransfield Strait (Fig. 1). This area is characterized by the confluence of the Bellingshausen Sea (comparatively warmer and less saline) and the Weddell Sea (colder and more saline). In addition, in the Bellingshausen Sea, the pattern of water masses with depth is usually characterized by a surface layer of cold Antarctic water over a layer of warmer circumpolar waters (Garcia et al., 2002).

The first cruise (ICEPOS 2004) took place from 14 January to 9 February 2004 aboard RV 'Las Palmas' and 12 stations were selected and sampled at 4 to 5 depths each, from surface waters to 150 m depth. These stations covered 3 transects: from Livingston Island to
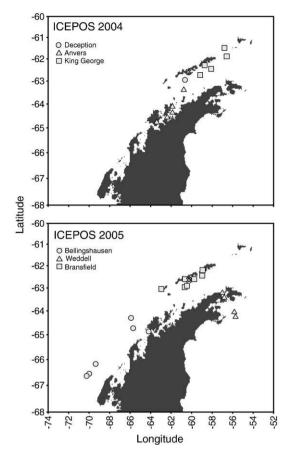

Fig. 1. Location of the stations sampled during ICEPOS 2004 and 2005 cruises. The study areas are represented using different symbols. The location of Livingston Island is marked by a cross symbol.

(1) Deception, (2) Anvers, and (3) King George islands (Fig. 1). The second cruise (ICEPOS 2005) took place aboard RV 'Hespérides' from 26 January to 26 February 2005. We selected 18 stations along the eastern Bellingshausen Sea, the Bransfield and Gerlache Straits, and the western Weddell Sea (Fig. 1). At each station, 5 to 6 depths were sampled, from surface waters to 150–200 m, below the deep chlorophyll maximum (DCM). Water was collected using a Niskin bottle with external spring (Ocean Test, 12 l) during ICEPOS 2004 and a SeaBird rossette sampler (24 Niskin bottles, 12 l each) attached to a SeaBird 25 conductivity/temperature/depth (CTD) system during ICEPOS 2005.

To describe CDOM geographical variability and controlling factors, sampling stations were merged into the different study areas following criteria of geographical proximity, water mass influence and similar physical and biological variables. The sampling stations during ICEPOS 2004 were divided into three study areas: (1) Deception Island (station #1), a semi-enclosed bay with high surface chl *a* concentration, (2) the transit to Anvers Island (stations #3–7), situated in the Western Bransfield Strait with influence from the Bellingshausen Sea and (3) the transit to King George Island (stations #8–12), in the Eastern Bransfield Strait with Weddell Sea influence. Likewise, the sampling stations during ICEPOS 2005 were grouped into three study areas: Bellingshausen Sea (stations #1–7), Antarctic Strait + Weddell Sea (referred as Weddell Sea, stations #8–11) and Bransfield Strait (stations #12–18).

2.2. Chemical and biological analyses

Water for CDOM optical characterization was filtered through precombusted Whatman GF/F filters and stored in polypropylene flasks at 4 °C in the dark prior to analysis (within a few hours). In each case,

the absorbance spectrum for the resultant filtrate was measured with a Shimadzu UV-2401 PC spectrophotometer using 10-cm quartz cuvettes. Absorbance scans from 250 to 700 nm were performed, a spectrum of MilliQ water filtered by GF/F and stored in parallel to the samples was subtracted as a baseline, and internal backscattering was corrected by subtracting the absorbance at 700 nm (Bricaud et al., 1981). Two selected wavelengths (325 and 443 nm) were expressed as Napierian absorption coefficients (a_{325} and a_{443}) in m^{-1} using the following equation (Miller, 1998):

$$a_{325, 443} = \frac{2.303 A_{325, 443}}{l} \tag{1}$$

where l is the optical pathlength in m and $A_{325, 443}$ is the spectrophotometric absorbance at 325 and 443 nm, respectively. We selected 325 nm as a reference wavelength within UVA spectrum (Nelson and Siegel, 2002) and 443 nm as it is the reference wavelength for satellite CDOM determinations. The spectral slopes between 275 and 295 nm ($S_{275-295}$) and between 350 and 400 nm ($S_{350-400}$) were calculated by a standard linear regression of the ln-transformed and the ratio of these slopes (S_R) was also calculated (Helms et al., 2008). Molar absorption coefficients ($m^2\,mol^{-1}$) were calculated as:

$$\varepsilon_{325, 443} = \frac{a_{325, 443}}{C} \tag{2}$$

where C is the concentration of DOC in $mmol\,l^{-1}$.

Samples for dissolved organic carbon (DOC) analyses were collected after filtration through pre-combusted Whatman GF/F filters into pre-combusted 10 ml glass ampoules, acidified with phosphoric acid (final pH<2), sealed and stored at 4 °C until analysis. DOC was analysed by high-temperature catalytic oxidation on a Shimadzu TOC-5000A. Standards of 44–45 µmol C l^{-1} and 2 µmol C l^{-1}, provided by D.A. Hansell and Wenhao Chen (Univ. of Miami), were used to assess the accuracy of the measurements.

Chl a concentration was determined fluorometrically (Parsons et al., 1984). Chl a concentration (µg l^{-1}) was converted to pigment absorption (a_{ph}, m^{-1}) using the following expression (Bricaud et al., 1995):

$$a_{ph}(443) = 0.04 \times Chla^{0.668} \tag{3}$$

Bacterial production (BP) was measured, only during ICEPOS 2005, through the incorporation of ^{3}H-Leucine using the technique proposed by Smith and Azam (1992). Bacterial abundance (BA) was determined by epifluorescence microscopy after DAPI staining (Porter and Feig, 1980) during ICEPOS 2004, and by flow cytometry after SYTO 13 staining (del Giorgio et al., 1996) during ICEPOS 2005. More details on these procedures can be found elsewhere (Ortega-Retuerta et al., 2008).

2.3. Data analyses

We determined the contribution of CDOM to non-water light attenuation at 443 nm as follows:

$$\%CDOM_{443} = \frac{a_{443}}{a_{ph443} + a_{443}} \times 100 \tag{4}$$

We used linear regression analyses to explore the relationship between CDOM and other physical and biological variables (salinity, DOC, chl a, BA and BP). We considered either all data together or segregated them by geographical areas prior to the analyses.

2.4. CDOM photoreactivity experiments

A total of 7 experiments were set up to determine CDOM photoreactivity rates in the study area. Water for the experiments during ICEPOS 2004 was collected from three different locations (near Livingston Island, Deception Island and Anvers Island), and two depths, surface (experiments #1, 2 and 4) and below the euphotic layer (50 m for Livingstone Island, and 150 m for Anvers Island, experiments #3 and 5). Table 1 shows the location and in situ properties of CDOM for each experiment. During ICEPOS 2005, two experiments were performed using waters from the deep chlorophyll maximum (DCM) from Bellingshausen (station #2) and Weddell (station #9) seas (experiments #6 and 7, respectively, Table 1).

Seawater was pre-filtered through pre-rinsed 0.2 µm nitrocellulose filters (Millipore) to exclude most, but not all bacteria (Hahn, 2004) and 8–12 50 ml-Quartz flasks (UV treatments). Then, 8–12 50 ml- black-tape covered flasks (dark treatments) were filled and incubated for 3 to 6 days in parallel on deck incubators flushed with surface seawater and receiving incident solar irradiance. A set of experimental bottles (two to three replicates for each treatment) were sequentially sampled 3 to 6 times over the incubation for CDOM characterization.

Incident UV was measured with a PUV 2500 Biospherical Instrument meter in experiments #2, 3, 4 and 5. Incident radiation data were not available for the rest of the experiments. Thus, we obtained data on incident radiation from Palmer Station (Anvers Island) provided by the NSF UV Monitoring Network, operated by Biospherical Instruments Inc. under a contract with the US National Science Foundation's Office of Polar Programs via Raytheon Polar Services Company. Data on UV from Palmer Station was within 14%, on average, of estimates derived at the location where the experiments were conducted.

Photobleaching kinetics usually fit negative exponential functions of the solar radiation dose or the exposure time (Reche et al., 1999). The net photobleaching coefficients ($k_{b\lambda}$) are defined as the slope of the ln-linear regression between absorption coefficients (a_λ) and the cumulative energy dose (D_n) (Eq. (5)) or the incubation time (t) ((Eq. (2))) in the quartz treatments:

$$a_{\lambda n} = a_{\lambda 0} e^{-k_b D_n} \tag{5}$$

Table 1

Location details, cumulative UV dose at 320 nm concentration of dissolved organic carbon (DOC), chlorophyll a (Chl a), bacterial abundance (BA), and absorption coefficients at 325 nm (a_{325}) and at 443 nm (a_{443}) of water used for the photoreactivity experiments.

Exp	Sampling area	Location	Depth	Salinity (PSU)	Cumulative UV dose at 320 nm (kJ m^{-2})	a_{325} (m^{-1})	a_{443} (m^{-1})	DOC (µmol L^{-1})	Chl a (µg l^{-1})	BA (×10^5 cell ml^{-1})
1	Deception Island	62° 57' S 60° 39' W	0 m	33.89	26.3	0.773	0.203	69.0	5.03	7.99
2	Livingston Island	63° 24' S 60° 23' W	0 m	nd	24.1	1.969	0.707	75.3	0.71	4.33
3	Livingston Island	63° 24´ S 60° 23' W	50 m	nd	24.1	0.738	0.234	70.5	0.64	3.80
4	Anvers Island	64° 35' S 63° 24' W	0 m	33.63	19.5	0.398	0.117	44.5	0.73	2.27
5	Anvers Island	64° 35' S 63° 24' W	150 m	34.14	19.5	0.776	0.252	54.9	0.35	2.50
6	Bellingshausen S.	66° 34' S 69° 60' W	DCM (40 m)	33.83	35.1	0.098	bdl	nd	0.64	2.25
7	Weddell Sea	64° 16' S 55° 43' W	DCM (80 m)	34.41	16.4	0.568	0.140	nd	4.42	12.5

bdl = below detection limit, nd = not determined.

Table 2
Mean and range (in parenthesis) values of physical and biological parameters for the different study geographical areas in the Southern Ocean and depths (upper mixed layer (UML) and below mixed layer (BML)) in 2004 and 2005.

Year	2004					
Area	Deception		Anvers		King George	
Depth	UML	BML	UML	BML	UML	BML
Temperature	1.27	−0.19	1.42	0.47	1.23	−0.58
(°C)	(0.93–1.65)		(0.92–2.18)	(0.11–0.81)	(0.89–1.48)	(−1.02–0.47)
Salinity	33.9	34.1	33.9	34.3	34.1	34.3
(PSU)			(33.6–34.0)	(34.1–34.4)	(34.0–34.7)	(34.2–34.4)
DOC	60	49	72	58	68	55
(μM)	(55–69)	(49–50)	(44–107)	(47–107)	(43–108)	(44–81)
Chl a[a]	5.92	0.71	0.61	0.30	0.84	0.08
(μg l^{-1})	(5.04–7.18)	(0.42–1.00)	(0.38–0.99)	(0.04–0.45)	(0.52–1.13)	(bdl–0.31)
BA[a]	8.57	na	3.14	1.87	3.58	1.56
(×10^5 cell ml^{-1})	(8.00–8.95)		(2.28–4.60)	(1.32–2.50)	(1.60–6.13)	(1.03–2.64)
BP[a]	na	na	na	na	na	na
(ng C l^{-1} h^{-1})						

Year	2005					
Area	Bellingshausen		Weddell	Bransfield		
Depth	UML	BML	Mixed layer	UML	BML	
Temperature	1.27	−0.09	−0.70	1.41	0.78	
(°C)	(0.77–1.51)	(−1.57–1.30)	(−1.09–1.48)	(1.29–1.56)	(0.33–1.29)	
Salinity	33.5	34.1	34.3	33.9	34.1	
(PSU)	(33.2–33.8)	(33.2–34.5)	(33.9–34.5)	(33.8–34.0)	(33.9–34.4)	
DOC	54	52	57	56	56	
(μM)	(45–62)	(44–58)	(49–77)	(48–65)	(47–67)	
Chl a[a]	1.21	0.29	1.98	2.95	0.91	
(μg l^{-1})	(0.55–2.19)	(0.01–1.27)	(0.25–4.71)	(0.99–5.36)	(0.10–2.24)	
BA[a]	6.13	3.41	7.99	12.25	8.35	
(×10^5 cell ml^{-1})	(1.55–16.2)	(0.57–7.78)	(3.45–16.6)	(5.78–17.6)	(5.04–13.9)	
BP[a]	26.8	8.45	55.7	36.20	17.55	
(ng C l^{-1} h^{-1})	(2.0–55.0)	(0.16–46.1)	(8.27–218)	(16.3–51.4)	(3.90–9.67)	

[a] Data from Ortega-Retuerta et al., 2008.

$$a_{\lambda n} = a_{\lambda 0} e^{-k_b t} \quad (6)$$

where λ is 325 or 443 nm, $a_{\lambda 0}$ and $a_{\lambda n}$ are the absorption coefficients measured at the initial and the final time, D_n is the cumulative sunlight dose at 320 nm and 400 nm in kJ m^{-2} and t is the time elapsed in days. Sunlight doses at 320 and 400 nm were chosen as the measurements at wavelengths closer to those for CDOM characterization (325 nm and 443 nm). The cumulative sunlight doses ranged from 16.4 to 28.4 kJ m^2 at 320 nm and from 60.23 to 104.8 kJ m^2 at 400 nm.

CDOM half lives (Eq. (7)) defined as the time for the initial absorption coefficients to decline by 50% (Reche and Pace, 2002) and

duplication times (Eq. (8)) as the time for the initial absorption coefficients to increase by 100% were calculated as:

$$hl_\lambda = \frac{\ln(0.5)}{k_{b\lambda}(d^{-1})} \quad (7)$$

$$dt_\lambda = \frac{1}{k_{b\lambda}(d^{-1})} \quad (8)$$

3. Results

In general, the stations situated in the Bellingshausen Sea were characterized by lower salinity than the stations located in the

Table 3
Mean values (± standard error) and ranges of absorption coefficients at 325 and 443 nm ($a_{325, 443}$, m^{-1}), molar absorption coefficients at 325 and 443 nm ($\varepsilon_{325, 443}$, m^2 mol^{-1}) and spectral slopes from 275 to 295 nm ($S_{275-295}$), and the ratio of the spectral slopes (S_R) in the six study areas. bdl = below detection limit, n = number of samples.

	a_{325} (m^{-1})	n	a_{443} (m^{-1})	n	ε_{325} (m^{-1})	n	ε_{443} (m^{-1})	n	$S_{275-295}$ (nm^{-1})	n	S_R	n
	Mean (range)		Mean (range)		Mean (range)		Mean (range)		Mean (range)		Mean (range)	
Total	0.36 ± 0.02 bdl–2.17	146	0.11 ± 0.01 bdl–0.76	143	6.12 ± 0.53 bdl–43.4	116	1.82 ± 0.20 bdl–15.2	113	0.019 ± 0.005 0.008–0.039	142	1.70 ± 0.04 0.53–3.36	140
Deception Island (2004)	1.30 ± 0.32 0.73–2.17	5	0.46 ± 0.11 0.25–0.76	5	24.8 ± 7.08 10.5–43.4	5	8.67 ± 2.50 3.64–15.2	5	0.018 ± 0.000 0.017–0.019	5	2.11 ± 0.11 2.06–2.15	5
Anvers I. transit (2004)	0.41 ± 0.07 0.09–1.28	20	0.13 ± 0.02 bdl–0.46	18	6.20 ± 1.07 0.91–11.3	17	2.20 ± 0.42 bdl–5.54	15	0.026 ± 0.001 0.018–0.037	20	2.09 ± 0.14 0.53–3.07	19
King George I. transit (2004)	0.18 ± 0.02 bdl–0.26	20	0.05 ± 0.01 bdl–0.14	19	2.97 ± 0.31 bdl–5.23	20	0.87 ± 0.16 bdl–3.03	19	0.029 ± 0.001 0.024–0.039	16	2.05 ± 0.16 0.92–3.36	15
Bellingshausen Sea (2005)	0.41 ± 0.02 0.22–0.66	38	0.14 ± 0.01 bdl–0.23	38	7.82 ± 0.53 3.88–13.5	23	2.57 ± 0.26 bdl–5.15	23	0.017 ± 0.000 0.012–0.019	38	1.84 ± 0.04 1.40–2.35	38
Weddell Sea (2005)	0.44 ± 0.03 0.19–0.76	24	0.10 ± 0.01 bdl–0.15	24	6.98 ± 0.38 3.62–10.3	18	1.68 ± 0.16 bdl–2.70	18	0.013 ± 0.000 0.011–0.016	24	1.28 ± 0.04 0.93–1.67	24
Bransfield Strait (2005)	0.23 ± 0.03 bdl–0.57	39	0.06 ± 0.01 bdl–0.19	39	4.20 ± 0.55 bdl–11.2	33	1.17 ± 0.20 bdl–3.72	33	0.014 ± 0.001 0.008–0.024	39	1.53 ± 0.01 0.98–2.70	39

Weddell Sea (Table 2). However, temperature profiles were more variable among areas. The stations located in the Bellingshausen Sea were characterized by shallow mixed layers (from 20 to 50 m) and increases in the temperature below the mixed layer depth. In contrast, the Weddell Sea stations exhibited mixed vertical profiles. Finally, the stations located along the Bransfield Strait had deeper mixed layers (from 70 to 100 m) or homogeneous depth profiles.

CDOM in the Southern Ocean showed similar average values in 2004 and 2005. The a_{325} values ranged from below the detection limit (0.046 m^{-1}) to 2.17 m^{-1} (mean ± SE 0.39 ± 0.06 m^{-1}) during ICEPOS 2004, with highest values inside Port Foster (a closed bay with high chl a) in Deception Island, and lowest in the transit to King George Island (Table 3). During ICEPOS 2005, the a_{325} values ranged from undetectable to 0.76 m^{-1} (mean ± SE 0.34 ± 0.02 m^{-1}). In
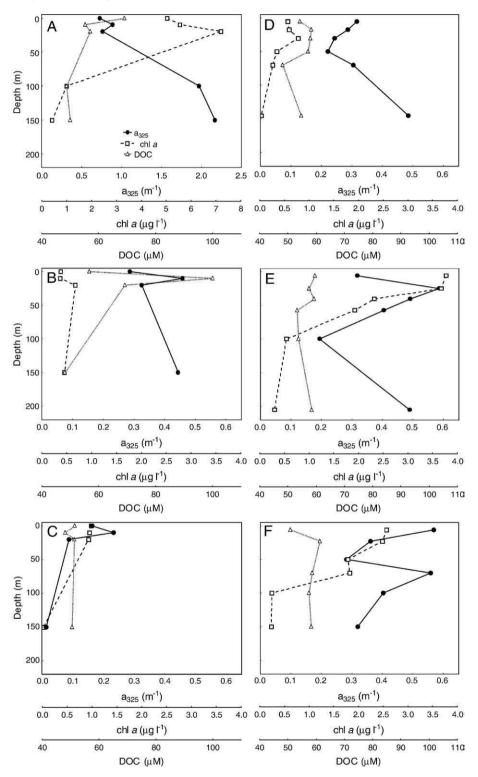

Fig. 2. Vertical profiles of absorption coefficients at 325 nm (a_{325}, m^{-1}, filled circles), chlorophyll a (chl a, µg l^{-1}, open squares) and dissolved organic carbon concentration (DOC, µmol l^{-1}, open triangles) in six representative locations: in Deception Island (A), the transit to Anvers Island (station #3, B) and the transit to King George Island (station #2, C) sampled in 2004, and the Eastern Bellingshausen Sea (station #4, D), the Western Weddell Sea (station #10, E) and the Bransfield Strait (station #12, F) sampled during 2005. Note the different scales.
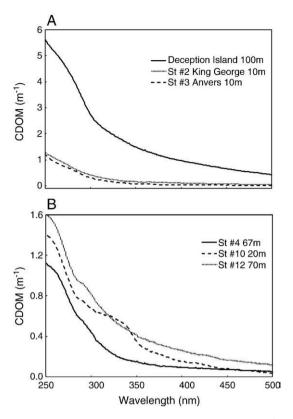
Fig. 3. Example spectra of absorption coefficients from 250 to 500 nm (m^{-1}) in same locations showed in Fig. 2.

2005, highest CDOM was observed within the polar circle in the Bellingshausen Sea (stations #2 and #3) and within the photic layer in the Weddell Sea, and lowest in the Bransfield Strait. The a_{443} values ranged from undetectable to 0.76 m^{-1} (mean ± SE 0.13 ± 0.03 m^{-1}) during 2004, and from undetectable to 0.23 m^{-1} (mean ± SE 0.11 ± 0.01 m^{-1}) during 2005. From all measurements, 24% were below the detection limit at 443 nm. CDOM vertical profiles were diverse (Fig. 2). In general, CDOM exhibited more geographical than interannual variability. In 5 out of 12 stations in 2004 and in 10 out of 18 stations in 2005, corresponding to western stations, CDOM values were higher in waters below 100 m than in the upper layer. This increase in CDOM with depth was particularly pronounced inside Deception Island (Fig. 2A), and in the stations situated in the Bellingshausen Sea (stations #1 to 7 in 2005, Fig. 2D). In contrast, CDOM showed higher values within the euphotic layer than below it in the transit to King George Island in 2004 (Fig. 2C) and in the Weddell Sea in 2005 (Fig. 2E). In the Bransfield Strait in 2005, no consistent vertical pattern was observed (Fig. 2F). A total of 11 stations out of 30 exhibited maxima of CDOM coinciding with chl a maxima.

DOC values ranged from 44 to 75 µM (mean value 55 µM) with little variation among areas (Table 2). DOC profiles were homogenous in 13 out of 26 stations, it decreased with depth in 10 stations located in the Bellingshausen Sea, and exhibited deep maxima in three stations situated near King George Island. Molar absorption coefficients ranged from undetectable to 43.4 m^2 mol^{-1} (mean ± SE 6.40 ± 0.71 m^2 mol^{-1}) at 325 nm (ε_{325}) and from undetectable to 15.2 m^2 mol^{-1} (mean ± SE 1.99 ± 0.51 m^2 mol^{-1}) at 443 nm (ε_{443}) (Table 3). These coefficients were highest in Deception Island and lowest in the transit to King George Island (Table 3), and vertical profiles generally tracked those of the absorption coefficients. The spectral slopes ($S_{275-295}$) ranged from 0.008 to 0.039 nm^{-1} and the values of S_R from 0.53 to 3.36 (Table 3). The lowest spectral slopes and ratios were observed in the Weddell Sea (Table 3). CDOM spectra from 250 nm to 500 nm fitted exponential models in all the study areas, with slight peaks at the UVA region of productive locations (Fig. 3).

Chlorophyll a showed a mean concentration of 0.73 ± 0.11 µg l^{-1} in 2004, excluding Port Foster within Deception Island where very high concentrations were detected (up to 7 µg l^{-1}), and a mean concentration of 2.15 ± 0.14 µg l^{-1} in 2005, with maxima in the Weddell Sea and Bransfield Strait. The pigment-specific absorption at 443 nm (a_{ph443}) ranged from 0.002 m^{-1} to 0.149 m^{-1} (mean 0.044 ± 0.002 m^{-1}). The contribution of CDOM to non-water light attenuation at 443 nm (%a_{cdom}(443)) was high (average 69%) ranging from 60% in the eastern area (King George Transit, Weddell Sea and Bransfield Strait) to 80% in the western area (Anvers Island transit and Bellingshausen Sea) (Fig. 4).

DOC and CDOM (a_{325}, a_{443}) were not significantly correlated ($p > 0.05$). In 2004, no significant relationships were obtained between CDOM (a_{325}, a_{443}) and salinity, chl a or bacterial abundance in the transit to Anvers Island. In contrast, a_{325} was significant and positively correlated to chl a in the stations in the transit to King George Island ($r = 0.54$, $p < 0.05$, $n = 20$). In the Bellingshausen Sea in 2005, significant negative relationships were observed only between a_{325} and chl a ($r = -0.42$, $p < 0.01$, $n = 38$) and BP ($r = -0.33$, $p < 0.05$, $n = 38$). In 2005, merging all data, we observed a significant and negative correlation between the spectral slopes ($S_{275-295}$) and the salinity (Fig. 5).

In particular, in the Weddell Sea positive relationships were observed between a_{325} and both chl a ($r = 0.49$, $p < 0.05$, $n = 24$, Fig. 6A) and BP ($r = 0.57$, $p < 0.01$, $n = 24$, Fig. 6B). In contrast, salinity was negatively correlated to a_{325} ($r = -0.64$, $p < 0.001$, $n = 22$, Fig. 6C).

3.1. CDOM photoreactivity experiments

The CDOM photoreactivity experiments showed CDOM net losses at 325 nm and 443 nm following exposure to the full spectrum of solar radiation (UV treatments) in 5 out of 7 experiments (Fig. 7), and increases in UV treatments in the other two experiments (exps. #3 and 6, Fig. 7). Subtle changes in CDOM were also observed in the dark treatments.
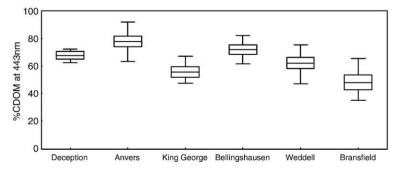

Fig. 4. Contribution in percentage of CDOM absorption at 443 nm with respect to total non-water absorption in the upper the mixed layer in the six study areas. Lines = Mean values, boxes = standard error and whiskers = non-outlier ranges.
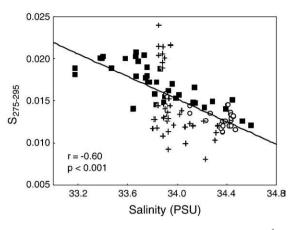
Fig. 5. Scatterplot between salinity (PSU) and spectral slopes ($S_{275-295}$, nm^{-1}) merging all data from ICEPOS 2005: Black squares: Bellingshausen Sea, white circles: Weddell Sea, crosses: Bransfield Strait. r = correlation coefficient; p = level of significance.

Daily changes in absorption coefficients were more pronounced at short wavelengths (Fig. 8). In 5 out of 7 experiments CDOM was reduced over sunlight exposure with decreases from 0.05 m^{-1} d^{-1} to -0.59 m^{-1} d^{-1} at 250 nm in the quartz treatments (Fig. 8A and B). We observed distinctive peaks below 300 nm in the CDOM spectra photogenerated in the experiments 1 and 7, those with the highest concentration of chl a and bacterial abundance in situ. In contrast, in the experiments 3 and 6 we observed subtle increases in CDOM over sunlight exposure (Fig. 8C).

The spectral slopes ($S_{275-295}$) and the S_R values exhibited a net increase over the incubation time in all experiments where photo-bleaching was the dominant process, whereas the slopes did not show this trend in the experiments 3 and 6 (Fig. 9).

Net photobleaching coefficients (k_{b325}) ranged from -0.02 to -0.07 (kJ m^{-2})$^{-1}$ and from -0.12 to -0.33 d^{-1} in those experiments where photobleaching was observed, corresponding to CDOM half lives ranging from 2.1 to 5.8 days (Table 4). In the experiments where photohumification was the dominant process (i.e. increases of CDOM over sunlight exposure), duplication times ranged from 10.9 to 15.7 days (Table 4). Net photobleaching coefficients at 443 nm (k_{443}) ranged from -0.006 to -0.018 (kJ m^{-2})$^{-1}$ and from -0.135 to -0.266 d^{-1}, corresponding to half lives from 2.6 to 5.1 days in the experiments displaying photobleaching, and duplication times from 4.9 to 10 days were calculated in the experiments with photohumi-fication (Table 5).

4. Discussion

CDOM values determined in this study are generally higher than those reported in the literature for the Southern Ocean (Table 6) or other areas of the ocean (Nelson et al., 1998; Siegel et al., 2002). However, the a_{325} values observed in this study are not substantially higher than those reported for the western Antarctic Peninsula area by Patterson (2000), and are in the range of reported values at the South Shetland Islands (Yocis et al., 2000). Other variables, such as chl a or bacterial abundance and production (Table 2) showed also relatively higher values than other ocean areas (e.g. <0.4 µg l^{-1} at the Australian sector (Clementson et al., 2001), 0.5–0.4 µg l^{-1} in Subantarctic area, (Howard-Williams et al., 1995)) indicative of the high productivity of this study area. Unfortunately, previous studies showing DOM optical properties in Antarctic productive areas (following algal blooms in the Ross Sea, with chl a averages higher than 1 µg l^{-1}, Barbini et al., 2003, Misic et al., 2006) are expressed in fluorescence units, making the comparison difficult. Also the mean contribution of CDOM to the total non-water absorption (68 %, Fig. 4) was also higher in the region investigated here than the average value
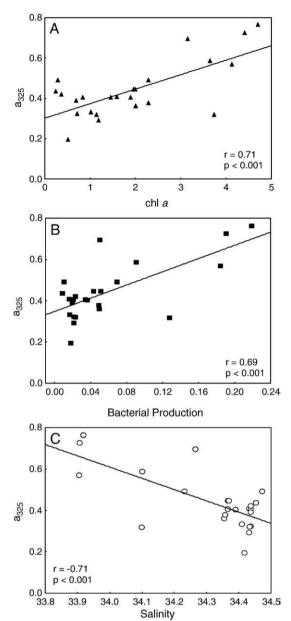

Fig. 6. Scatterplots between chlorophyll a (chl a , µg l^{-1}) (A), bacterial production (BP, µg C l^{-1} h^{-1}) (B) and salinity (PSU) (C) and a_{325} (m^{-1}) in the Weddell Sea area of the Southern Ocean. r = correlation coefficient; p = level of significance.

for the ocean surface (46%, Siegel et al., 2002), highlighting the remarkable role of CDOM regulating light attenuation in these waters.

CDOM vertical distribution did not follow a common pattern in all the study stations. Similar results have been reported in the literature, from maxima of CDOM in surface waters (Misic et al., 2006) to low CDOM concentrations within the first 200–300 m (Wedborg et al., 1998; Yamashita et al., 2007). The CDOM profiles appear to be variable across oceans, from high CDOM at the surface at high latitudes (e.g. Kitidis et al., 2006) to surface depletion of CDOM at lower latitudes (Nelson et al., 1998, Kitidis et al., 2006). The absence of strong relationships, merging all data, between CDOM and DOC and biological variables at the scales investigated, underlines the com-plexity of CDOM distribution. In the Western Antarctic Peninsula area (the transit to Anvers Island in 2004 and Bellingshausen Sea stations in 2005), variability in CDOM was independent of chlorophyll a and bacteria patterns. The vertical distribution, with particularly high CDOM below the upper mixed layer, suggests that CDOM can be dominated mostly by physical forces. In these stations, with well-
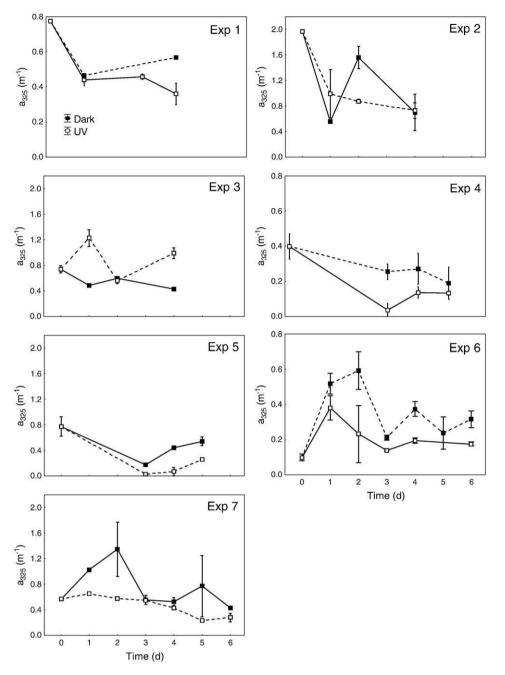
Fig. 7. Changes in absorption coefficients at 325 nm (a_{325}, m^{-1}) over time (days) in all photoreactivity experiments. Open squares = UV treatments. Filled squares = dark treatments. Whiskers = standard error. Note the different scales in the y axis.

stratified water columns and a shallow mixed layer, the upper mixed layer is depleted in CDOM likely due to photobleaching losses. In waters below the mixed layer, high CDOM can be explained, in addition to the absence of photobleaching, by physical transport as this area is influenced by relatively warm waters from the Antarctic circumpolar current (Garcia et al., 2002; Smith et al., 1999).

In particular, in the Weddell Sea stations, where water was collected in areas surrounded by large icebergs, the negative relationship between CDOM and salinity signals a possible role of ice melting as a source of CDOM, consistent with previous literature (Kieber et al., 2009). CDOM in ice can result from a mixture of trapped terrestrial material and biological processes (Stedmon et al., 2007). Although previous studies have discarded ice as a dominant source of DOM (Skoog et al., 2005), high absorbance has been measured in ice cores at the Weddell Sea (a_{440} up to 7.60 m^{-1}, D.N. Thomas pers. comm.). This source can also be indirect through the growth of algae

and bacterial activity associated to nutrient release during ice melting. Indeed, a previous study has demonstrated CDOM generation linked to bacterial activity in this area (Ortega-Retuerta et al., 2009). Therefore, these links could explain the significant correlations between salinity, chl a and bacterial production in this area (Fig. 5).

In this study we chose the use of slope values derived from the shortest band of the spectrum to increase precision (Helms et al., 2008). However, spectral slope values can be highly variable according to the spectral wavelengths used or the regression technique applied (i.e. linear vs. non-linear model II regression), making comparison among studies difficult (Nelson and Siegel, 2002). The negative relationship between $S_{275-295}$ and salinity appears to indicate the presence of low molecular weight DOM in our low salinity samples (Helms et al., 2008). This relationship was only encountered during 2005, whereas no significant relationship was found in 2004, presumably because sampling was performed earlier in the season.
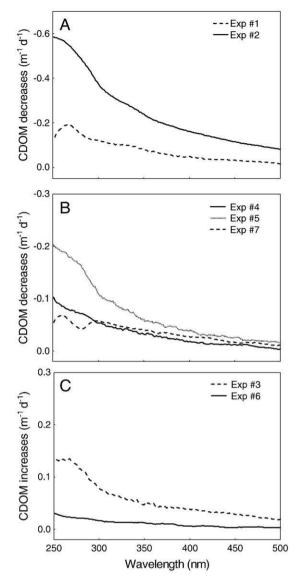
Fig. 8. Daily changes in the CDOM spectra from 250 to 500 nm in all experiments.

Fig. 9. Changes in spectral slopes ($S_{275-295}$, nm^{-1} and S_R,) over time (days) in photoreactivity experiments #1 (Deception Island 0 m, A), exp #4 (Anvers Island 0 m, B) and exp #6 (Bellingshausen Sea DCM, C). Open squares = UV treatments. Filled squares = dark treatments. Whiskers = standard error.

In 2004, lower values of chl *a* and bacterial abundance were observed, and the effects of ice melting were still little pronounced.

The results of the photoreactivity experiments demonstrate the complexity of CDOM photoreactions in marine systems. We observed both photobleaching and photohumification of CDOM, inducing changes in CDOM within days (Tables 4, 5, Fig. 8). Photobleaching appears to be the dominant process involved in CDOM transformations as it occurred in 5 of 7 experiments, and photobleaching coefficients lead to CDOM half lives in the order of a few days. These results are consistent with previous experimental studies in this area reporting significant losses of absorption in less than 24 h (Bertilsson et al., 2004; Kieber and Mopper, 1995; Obernosterer et al., 2001). The increases in the spectral slopes along with photobleaching were consistent with previous works (Del Vecchio and Blough, 2002; Reche et al., 2001) and, in particular, the $S_{275-295}$ and S_R values (Helms et al., 2008). However, the increases in slopes along with irradiation in the experiments were not accompanied consistently by higher slopes at the surface in the field stations, where CDOM quality (i.e. slope and ratios) may be submitted to greater complexity. Although we observed some changes in CDOM over incubation time also in the dark, we generally detected larger declines in CDOM when exposed to the full spectrum of solar radiation. Despite that CDOM decreased over
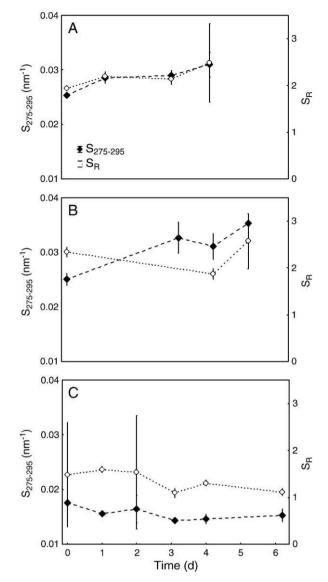
the whole incubations in 5 experiments, the increase in CDOM observed in some of the experiments (e.g. the experiments 4 and 5), generally starting after 3 days, could be attributed to bacterial activity that can generate CDOM. Unfortunately, this contribution cannot be quantified since bacterial growth was not monitored in these experiments. The absence of net photobleaching in two of the experiments (experiments #3 and 6) can be attributable to a resistance of CDOM from these sites to photobleaching or, alternatively, to lower incident radiation during the experiments than those recorded at Palmer station. Although in situ irradiance measurements were not available for the experiment 6, cloudy days during the incubation suggest lower cumulative sunlight doses than estimated. In the experiment 6, performed using waters from Bellingshausen Sea, we observed increase of absorption both in UV and dark treatments, but the lower increase in absorption in the UV treatments than in dark treatments suggests that CDOM photobleaching was occurring, which could explain the lower CDOM observed in surface waters of Bellingshausen Sea stations.

The experiments highlight photobleaching as a significant sink of CDOM, acting at time scales of days (half lives 2.1 to 5.8 days). This

Table 4
Net photoreactivity coefficient rates (k) (mean ± standard error) expressed in sunlight dose $((kJ\,m^2)^{-1})$ and time (d^{-1}) units and half lives (photobleaching) or duplication times (photohumification) (d) at 325 nm determined in the experiments.

Exp	Sampling area	Depth	Process	$k_{325}\,(kJ/m^2)^{-1}$	$k_{325}\,(d^{-1})$	Half life$_{325}$ (d)	Duplication time$_{325}$ (d)
1	Deception Island	0 m	Photobleaching	-0.02 ± 0.01	-0.12 ± 0.05	5.8	
2	Livingston Island	0 m	Photobleaching	-0.03 ± 0.01	-0.20 ± 0.07	3.5	
3[a]	Livingston Island	50 m	Photohumification	0.01 ± 0.00	0.07 ± 0.02		15.7
4	Anvers Island	0 m	Photobleaching	-0.04 ± 0.01	-0.23 ± 0.07	3.0	
5	Anvers Island	150 m	Photobleaching	-0.07 ± 0.04	-0.33 ± 0.21	2.1	
6[a]	Bellingshausen S.	DCM (40 m)	Photohumification	0.02 ± 0.00	0.09 ± 0.01		10.9
7	Weddell Sea	DCM (80 m)	Photobleaching	-0.04 ± 0.01	-0.15 ± 0.04	4.7	

[a] The calculation in these experiments only considered the initial and final time.

Table 5
Net photoreactivity coefficient rates in sunlight dose $((kJ\,m^2)^{-1})$ and in time (d^{-1}) units and half lives (photobleaching) and duplication times (photohumification) (d) at 443 nm determined in the experiments.

Exp	Sampling area	Depth	Process	$k_{443}\,(kJ/m^2)^{-1}$	$k_{443}\,(d^{-1})$	Half life$_{443}$ (d)	Duplication time$_{443}$ (d)
1	Deception Island	0 m	Photobleaching	-0.006 ± 0.004	-0.135 ± 0.095	5.1	
2	Livingston Island	0 m	Photobleaching	-0.014 ± 0.003	-0.266 ± 0.077	2.6	
3[a]	Livingston Island	50 m	Photohumification	0.005 ± 0.001	0.103 ± 0.019		10.0
4	Anvers Island	0 m	Photobleaching	-0.018 ± 0.006	-0.252 ± 0.084	2.8	
5	Anvers Island	150 m	Photobleaching	-0.017 ± 0.008	-0.249 ± 0.118	2.8	
6[a]	Bellingshausen S.	DCM (40 m)	Photohumification	0.013 ± 0.003	0.215 ± 0.050		4.9
7	Weddell Sea	DCM (80 m)	Photobleaching	-0.014 ± 0.006	-0.203 ± 0.060	3.4	

[a] The calculation in these experiments only considered the initial and final time.

explained the lower CDOM values frequently found in surface waters. Indeed, those stations with shallower mixed layers and more defined stratification (e.g. stations in the Bellingshausen Sea) generally exhibited lower CDOM at the surface, while at stations with mixed profiles (e.g. the ones located in the Weddell Sea and Bransfield Strait) we did not observe these CDOM minima at the surface. Alternatively, photohumification may represent a source of CDOM in clear waters, but at longer time scales of between 11 and 16 days. Indeed, the proposed mechanism for photohumification is an enhanced cross-linking of humic substances by photogenerated aldehydes (Kieber et al., 1997), which needs a previous photodegradation step to release these aldehydes. Our experiments are able to track the net result of phototransformations of CDOM where the two processes, photobleaching and photohumification are likely to occur simultaneously although with different strength. The reported photobleaching coefficients are based on surface irradiance, so the attenuation of UV in the water column would presumably yield lower changes in CDOM associated to photoreactions decrease. However, the penetration of UV radiation through the water column in the study area and sampling time (up to 21 m, S. Agusti unpublished data) were generally shallower than the mixed layer depth. Therefore, mixing within the upper layer would result in enhanced CDOM photoreactions (Whitehead et al., 2000). In addition to phototransformations,

biogeneration by bacteria and krill is an important source of CDOM in this area of the Southern Ocean (Ortega-Retuerta et al., 2009) that can, to some extent, counteract the losses due to photobleaching.

In summary, the high CDOM values reported in our study support the existence of a global trend toward increasing CDOM with latitude, and are also in agreement with local conditions of high productivity in the Antarctic Peninsula region. We demonstrate the strong photoreactive nature of CDOM in timescale of days and identify a significant relationship between salinity and CDOM absorption and optical quality in this region of the Southern Ocean.

Acknowledgements

Table 6
Comparative values of CDOM absorption coefficients (average and/or ranges) previously reported in the literature for the study region.

Study area	Wavelength (nm)	$a_{CDOM}\,(m^{-1})$	Reference
Antarctic Peninsula	443	0.11 (bdl–0.76)	This study
Antarctic Peninsula	320	0.39 (bdl–2.30)	This study
Antarctic Peninsula	400	0.15 (bdl–1.07)	This study
Weddell-Scotia confluence (Ant. Pen.)	300	0.19–0.62	Yocis et al. (2000)
Western Ant. Pen.	320	0.13 (bdl–0.77)	Patterson (2000)
Australasian sector	443	0.019–0.099	Clementson et al. (2001)
Ross Sea	400	0.02–0.12	Reynolds et al. (2001)
Ross Sea	443	0.014–0.054	Kieber et al. (2009)
Subantarctic	443	0.027–0.033	Howard-Williams et al. (1995)

References

Amon, R.M.W., Benner, R., 1994. Rapid cycling of high-molecular-weight dissolved organic matter in the ocean. Nature 369 (6481), 549–552.

Babin, M., et al., 2003. Variations in the light absorption coefficients of phytoplankton, nonalgal particles, and dissolved organic matter in coastal waters around Europe. J. Geophys. Res. Oceans 108 (C7), 20.

Barbini, R., Colao, F., Fantoni, R., Ferrari, G.M., Lai, A., Palucci, A., 2003. Application of a lidar fluorosensor system to the continuous and remote monitoring of the Southern Ocean and Antarctic Ross Sea: results collected during the XIII and XV Italian oceanographic campaigns. Int. J Remote Sens. 24 (16), 3191–3204.

Bertilsson, S., Carlsson, P., Graneli, W., 2004. Influence of solar radiation on the availability of dissolved organic matter to bacteria in the Southern Ocean. Deep-Sea Res. II 51 (22–24), 2557–2568.

Biers, E.J., Zepp, R.G., Moran, M.A., 2007. The role of nitrogen in chromophoric and fluorescent dissolved organic matter formation. Mar. Chem. 103, 46–60.

Blough, N.V., del Vecchio, R., 2002. Chromophoric DOM in the coastal environment. In: Hansell, D.A., Carlson, C.A. (Eds.), Biogeochemistry of Marine Dissolved Organic Matter. Academic Press, San Diego, pp. 547–578.

Bricaud, A., Morel, A., Prieur, L., 1981. Absorption by dissolved organic matter of the sea (yellow substance) in the UV and visible domains. Limnol. Oceanogr. 26 (1), 43–53.

Bricaud, A., Babin, M., Morel, A., Claustre, H., 1995. Variability in the chlorophyll-specific absorption coefficients of natural phytoplankton: analysis and parameterization. J. Geophys. Res. Oceans 100 (C7), 13321–13332.

Cammack, W.K.L., Kalff, J., Prairie, Y.T., Smith, E.M., 2004. Fluorescent dissolved organic matter in lakes: relationships with heterotrophic metabolism. Limnol. Oceanogr. 49 (6), 2034–2045.

Carder, K.L., Steward, R.G., Harvey, G.R., Ortner, P.B., 1989. Marine humic and fulvic-acids — their effects on remote-sensing of ocean chlorophyll. Limnol. Oceanogr. 34 (1), 68–81.

Chen, R.F., Bada, J.L., 1992. The fluorescence of dissolved organic matter in seawater. Mar. Chem. 37 (3–4), 191–221.

Clementson, L.A., Parslow, J.S., Turnbull, A.R., McKenzie, D.C., Rathbone, C.E., 2001. Optical properties of waters in the Australasian sector of the Southern Ocean. J. Geophys. Res. Oceans 106 (C12), 31611–31625.

Coble, P.G., 2007. Marine optical biogeochemistry: the chemistry of ocean color. Chem. Rev. 107 (2), 402–418.

Del Giorgio, P., Bird, D.F., Prairie, Y.T., Planas, D., 1996. Flow cytometric determination of bacterial abundance in lake plankton with the green nucleic acid stain SYTO 13. Limnol. Oceanogr. 41 (4), 783–789.

Del Vecchio, R., Blough, N.V., 2002. Photobleaching of chromophoric dissolved organic matter in natural waters: kinetics and modeling. Mar. Chem. 78 (4), 231–253.

Ferrari, G.M., 2000. The relationship between chromophoric dissolved organic matter and dissolved organic carbon in the European Atlantic coastal area and in the West Mediterranean Sea (Gulf of Lions). Mar. Chem. 70 (4), 339–357.

Garcia, M.A., Castro, C.G., Rios, A.F., Doval, M.D., Roson, G., Gomis, D., Lopez, O., 2002. Water masses and distribution of physico-chemical properties in the Western Bransfield Strait and Gerlache Strait during Austral summer 1995/96. Deep-Sea Res. II 49 (4–5), 585–602.

Hahn, M.W., 2004. Broad diversity of viable bacteria in 'sterile' (0.2 μm) filtered water. Res. Microbiol. 155 (8), 688–691.

Hansell, D.A., Carlson, C.A., 2002. Biogeochemistry of Marine Dissolved Organic Matter. Academic Press, San Diego.

Helms, J.R., Stubbins, A., Ritchie, J.D., Minor, E.C., Kieber, D.J., Mopper, K., 2008. Absorption spectral slopes and slope ratios as indicators of molecular weight, source, and photobleaching of chromophoric dissolved organic matter. Limnol. Oceanogr. 53, 955–969.

Howard-Williams, C., Davies-Colley, R., Vincent, W.F., 1995. Optical properties of the coastal and oceanic waters off South Island, New Zealand: regional variation. N.Z. J. Mar. Freshw. Res. 29, 589–602.

Kalle, K., 1966. The problem of gelbstoff in the sea. Oceanogr. Mar. Biol. Annu. Rev. 4, 91–104.

Kieber, D.J., Mopper, K., 1995. Photochemistry of Antarctic waters during the 2004 austral summer. Antarc. J. U.S. 30 (5), 150–151.

Kieber, D.J., McDaniel, J., Mopper, K., 1989. Photochemical source of biological substrates in seawater: implications for carbon cycling. Nature 341 (6243), 637–639.

Kieber, R.J., Hydro, L.H., Seaton, P.J., 1997. Photooxidation of triglycerides and fatty acids in seawater: implication toward the formation of marine humic substances. Limnol. Oceanogr. 42 (6), 1454–1462.

Kieber, R.J., Li, A., Seaton, P.J., 1999. Production of nitrite from the photodegradation of dissolved organic matter in natural waters. Environ. Sci. Technol. 33 (7), 993–998.

Kieber, D.J., Toole, D.A., Kiene, R.P., 2009. Chromophoric dissolved organic matter cycling during a Ross Sea *Phaeocystis antarctica* bloom. Smithsonian at the Poles: Contributions to International Polar Year Science — a Smithsonian Contribution to Knowledge. Smithsonian Inst, Washington, DC, pp. 319–333.

Kitidis, V., et al., 2006. Variability of chromophoric organic matter in surface waters of the Atlantic Ocean. Deep Sea Res. II 53 (14–16), 1666–1684.

Miller, W.L., 1998. Photochemical principles and experimental considerations. In: Hessen, D.O., Tranvik, L.J. (Eds.), Aquatic Humic Substances: Ecology and Biogeochemistry. Springer, Berlin, pp. 125–143.

Misic, C., Castellano, M., Ruggieri, N., Povero, P., 2006. Dissolved organic matter characterisation and temporal trends in Terra Nova Bay (Ross Sea, Antarctica). Estuar. Coast. Shelf Sci. 70 (3), 405–414.

Mopper, K., et al., 1991. Photochemical degradation of dissolved organic carbon and its impact on the oceanic carbon cycle. Nature 353 (6339), 60–62.

Nelson, N.B., Siegel, D.A., 2002. Chromophoric DOM in the open ocean. In: Hansell, D.A., Carlson, C.A. (Eds.), Biogeochemistry of Marine Dissolved Organic Matter. Academic Press, San Diego.

Nelson, N.B., Siegel, D.A., Michaels, A.F., 1998. Seasonal dynamics of colored dissolved material in the Sargasso Sea. Deep-Sea Res. I 45 (6), 931–957.

Nelson, N.B., Carlson, C.A., Steinberg, D.K., 2004. Production of chromophoric dissolved organic matter by Sargasso Sea microbes. Mar. Chem. 89 (1–4), 273–287.

Obernosterer, I., Sempere, R., Herndl, G.J., 2001. Ultraviolet radiation induces reversal of the bioavailability of DOM to marine bacterioplankton. Aquat. Microb. Ecol. 24 (1), 61–68.

Opsahl, S., Benner, R., 1998. Photochemical reactivity of dissolved lignin in river and ocean waters. Limnol. Oceanogr. 43 (6), 1297–1304.

Ortega-Retuerta, E., Reche, I., Pulido-Villena, E., Agustí, S., Duarte, C.M., 2008. Exploring the relationship between active bacterioplankton and phytoplankton in the Southern Ocean. Aquat. Microb. Ecol. 52 (1), 99–106.

Ortega-Retuerta, E., Frazer, T.K., Duarte, C.M., Ruiz-Halpern, S., Tovar-Sánchez, A., Arrieta, J.M. and Reche, I., 2009. Biogeneration of chromophoric dissolved organic matter by bacteria and krill in the Southern Ocean. Limnol. Oceanogr. 54 (6), 1941–1950.

Parsons, T.R., Maita, Y., Lalli, C.M., 1984. A Manual of Chemical and Biological Methods for Sea Water Analysis. Pergamon Press, Oxford.

Patterson, K.W., 2000. Contribution of chromophoric dissolved organic matter to attenuation of ultraviolet radiation in three contrasting coastal areas, PhD University of California Santa Barbara, USA.

Porter, K.G., Feig, Y.S., 1980. The use of DAPI for identifying and counting aquatic microflora. Limnol. Oceanogr. 25 (5), 943–948.

Reche, I., Pace, M.L., 2002. Linking dynamics of dissolved organic carbon in a forested lake with environmental factors. Biogeochem. 61 (1), 21–36.

Reche, I., Pace, M.L., Cole, J.J., 1999. Relationship of trophic and chemical conditions to photobleaching of dissolved organic matter in lake ecosystems. Biogeochem. 44 (3), 259–280.

Reche, I., Pulido-Villena, E., Conde-Porcuna, J.M., Carrillo, P., 2001. Photoreactivity of dissolved organic matter from high-mountain lakes of Sierra Nevada, Spain. Arct. Antarct. Alp. Res. 33 (4), 426–434.

Reynolds, R.A., Stramski, D., Mitchell, B.G., 2001. A chlorophyll-dependent semianalytical reflectance model derived from field measurements of absorption and backscattering coefficients within the Southern Ocean. J. Geophys. Res.-Oceans 106 (C4), 7125–7138.

Rochelle-Newall, E.J., Fisher, T.R., 2002. Production of chromophoric dissolved organic matter fluorescence in marine and estuarine environments: an investigation into the role of phytoplankton. Mar. Chem. 77 (1), 7–21.

Santschi, P.H., Santschi, P.H., Guo, L.D., Baskaran, M., Trumbore, S., Southon, J., Bianchi, T.S., Honeyman, B., Cifuentes, L., 1995. Isotopic evidence for the contemporary origin of high molecular weight organic matter in oceanic environments. Geochim. Cosmochim. Acta 59 (3), 625–631.

Siegel, D.A., Maritorena, S., Nelson, N.B., Hansell, D.A., Lorenzi-Kayser, M., 2002. Global distribution and dynamics of colored dissolved and detrital organic materials. J. Geophys. Res. Oceans 107 (C12), 3228. doi:10.1029/2001JC000965.

Siegel, D.A., Maritorena, S., Nelson, N.B., 2005. Independence and interdependencies among global ocean color properties: reassessing the bio-optical assumption. J. Geophys. Res. Oceans 110, C07011. doi:10.1029/2004JC002527.

Skoog, A., Wedborg, M., Lara, R., Kattner, G., 2005. Spring distribution of dissolved organic matter in a system encompassing the Northeast Water Polynya: implications for early-season sources and sinks. Mar. Chem. 94 (1–4), 175–188.

Smith, D.C., Azam, F., 1992. A simple economical method for measuring bacterial protein synthesis rates in seawater using 3H leucine. Mar. Microb. Food Webs 6, 107–114.

Smith, R.C., Prezelin, B.B., Baker, K.S., Bidigare, R.R., Boucher, N.P., Coley, T., Karentz, D., Macintyre, S., Matlick, H.A., Menzies, D., Ondrusek, M., Wan, Z., Waters, K.J., 1992. Ozone depletion: ultraviolet radiation and phytoplankton biology in Antarctic waters. Science 255 (5047), 952–959.

Smith, D.A., Hofmann, E.E., Klinck, J.M., Lascara, C.M., 1999. Hydrography and circulation of the West Antarctic Peninsula continental shelf. Deep-Sea Res. I 46 (6), 925–949.

Stedmon, C.A., et al., 2007. Characteristics of dissolved organic matter in Baltic coastal sea ice: allochthonous or autochthonous origins? Environ. Sci. Technol. 41 (21), 7273–7279.

Twardowski, M.S., Donaghay, P.L., 2001. Separating in situ and terrigenous sources of absorption by dissolved materials in coastal waters. J. Geophys. Res.-Oceans 106 (C2), 2545–2560.

Vaughan, D.G., et al., 2003. Recent rapid regional climate warming on the Antarctic Peninsula. Clim. Change 60 (3), 243–274.

Vodacek, A., Blough, N.V., DeGrandpre, M.D., Peltzer, E.T., Nelson, R.K., 1997. Seasonal variation of CDOM and DOC in the Middle Atlantic Bight: terrestrial inputs and photooxidation. Limnol. Oceanogr. 42 (4), 674–686.

Wedborg, M., Hoppema, M., Skoog, A., 1998. On the relation between organic and inorganic carbon in the Weddell Sea. J. Mar. Syst. 17 (1–4), 59–76.

Whitehead, R.F., de Mora, S., Demers, S., Gosselin, M., Monfort, P., Mostajir, B., 2000. Interactions of ultraviolet-B radiation, mixing, and biological activity on photobleaching of natural chromophoric dissolved organic matter: a mesocosm study. Limnol. Oceanogr. 45 (2), 278–291.

Williams, P.M., 1971. The distribution and cycling of organic matter in the ocean. In: Faust, S.D., Hunter, J.V. (Eds.), Organic Compounds in the Aquatic Environment. Dekker, New York, pp. 145–163.

Yamashita, Y., Tsukasaki, A., Nishida, T., Tanoue, E., 2007. Vertical and horizontal distribution of fluorescent dissolved organic matter in the Southern Ocean. Mar. Chem. 106 (3–4), 498–509.

Yocis, B.H., Kieber, D.J., Mopper, K., 2000. Photochemical production of hydrogen peroxide in Antarctic waters. Deep-Sea Res. I 47 (6), 1077–1099.